Int. J. Electrochem. Sci., 8 **(2013)** 10672 - 10687

International Journal of
ELECTROCHEMICAL
SCIENCE
www.electrochemsci.org

Synthesis and Characterizations of BSCF at Different pH as Future Cathode Materials for Fuel Cell

Farhanini Yusoff[1], *Azizan Aziz*[2], *Norita Mohamed*[1], *Sulaiman Ab Ghani*[1*]

[1]Pusat Pengajian Sains Kimia, Universiti Sains Malaysia, 11800 USM, Pulau Pinang, Malaysia
[2]Pusat Pengajian Kejuruteraan Bahan & Sumber Mineral, Universiti Sains Malaysia, Seri Ampangan, 14300 Nibong Tebal, Pulau Pinang, Malaysia
[*]E-mail: sag@usm.my

Received: 22 April 2013 / *Accepted:* 3 July 2013 / *Published:* 1 August 2013

The synthesis of $Ba_{0.5}Sr_{0.5}Co_{0.8}Fe_{0.2}O_{3-\delta}$ (BSCF) using citrate-EDTA complexing method was carried out at pH 5, 7 and 9. Their suitability as cathode materials for intermediate temperature solid oxide fuel cells (SOFC) was investigated. The BSCF solutions was heated to 100 °C yielding a metal-citrate-nitrate gel complex precursor which was later calcined at 1000 °C for a period of 4 hours to produce the BSCF powder. The X-ray diffraction pattern of the calcined powder showed that it had undergone a complete phase formation. It was found that the pH value was crucial for the chelation process as well as for the purity of the phase obtained. The BSCF with a compact particle arrangement was obtained at pH 9. The nitrogen adsorption studies indicated that the BSCF powders had a mixture of microporous and mesoporous particles. Analysis by thermogravimetry revealed that the weight loss resulted from the oxygen-releasing capacity of the BSCF structure. The largest surface area was observed for BSCF powders prepared at pH 9. The BSCF at pH 9 prepared at various solution volumes was deposited on a glassy carbon electrode and characterized electrochemically. Cyclic voltammograms showed that the amount of BSCF deposited influenced the electron transfer, mass transport and capacitance behavior. Electrochemical impedance spectroscopy indicated that the electrode process was favorable.

Keywords: Adsorption; BSCF; Modified electrode; pH; Porosity

1. INTRODUCTION

Mixed ionic-electronic conductors with a perovskite oxide structure are popular materials of choice for solid oxide fuel cell (SOFC) cathodes, catalysts, and also as oxygen permeable membrane [1-3]. One such perovskite is $Ba_{0.5}Sr_{0.5}Co_{0.8}Fe_{0.2}O_{3-\delta}$ (BSCF) which has attracted great interest among researchers owing to its ultrahigh oxygen permeability and favorable structural stability [4].

Accordingly, BSCF has been proven to be a good material for solid SOFC cathode [5-7]. They have appealing properties, such as ionic conductivity, superconductivity, magneto-resistance and ferro-electricity.

A variety of models have been developed to describe the reaction mechanisms of SOFC cathode [8-9]. However, many important issues like the transport of oxygen and electrode kinetics have not yet been resolved. It is generally agreed that the cathode reaction of a SOFC is an electrochemical process involving chargeable particles. But, since the reaction occurs initially at the cathode surface the surface overpotential should be an important factor to the entire cathode reaction process [10].

The oxygen reduction step at the cathode is currently one of the main contributors to the total cell resistance. Any enhancements of the catalytic activity of the cathode would have a strong impact on the final fuel cell power density. Therefore, the development of cathode materials for the enhancement of electrocatalytic activity is of critical importance for an SOFC. A cathode should also have high electrical conductivity other than having high electrocatalytic activity for the oxygen reduction reaction. Thus, a favorable cathode should have high oxygen exchange capacities and diffusivity for easy incorporation of oxygen ions and for fast transport of the oxygen ions within its lattice respectively [11].

The search to overcome the above mentioned problem is still a challenge. But one promising concept that may improve oxygen exchange and diffusion on the cathode surface layer is by increasing the porosity of BSCF cathode. The enhancement of fuel cell performance by porous cathodes has been reported [12]. Porous cathodes provide better dispersion of the gases to unexposed areas, hence, increasing the oxygen reduction reaction. By optimizing the porosity of cathode, reduction area available for oxygen gas will be larger. Therefore, the electrocatalytic activity is increased and higher current density will be generated within the cell.

The combined EDTA–citrate method appears to be one of the most widely employed method for the synthesis of BSCF. It is a complex synthesis that can be tailored by the pH value used [1]. The advantage of this method is that all the reactants are mixed in a solution at a molecular level. Thus, it will lead to more homogeneous reaction products with low energy requirements and faster reaction rates [13-17]. The pH of the precursor solution is the important factor for controlling the powder morphology and crystal structure development [18]. To date, no research has been done to investigate the correlation between the pH value and porosity of BSCF. This study shows that the physical properties, e.g. density and porosity, of a BSCF powder will vary with the pH used for its preparation.

2. MATERIALS AND METHOD

2.1. Reagents and equipments

Ethylenediamminetetraacetic acid (EDTA), potassium ferrocyanide (99.0 %), potassium chloride (99.0 %), anhydrous citric acid and nitrate salts of barium (II), strontium (II), cobalt (II) and iron (III) were purchased from Sigma Aldrich, USA and were used as received. Ammonia solution was purchased from Systerm Chemicals, Australia. Solutions were prepared with water from Millipore Direct – Q3 (18.2 MΩcm) of Millipore, USA.

X-ray diffraction (XRD) measurements were performed using an X-ray diffractometer, Siemens-D5000, Germany. Thermogravimetric analyses (TGA) were performed with a thermal analyzer Pyris 1 of Perkin Elmer, USA. The Brunauer-Emmett-Teller (BET) surface area and porosity properties were measured using multi point BET Quantachrome surface area analyzer of NovaWin 32, USA. The surface morphologies of the samples were characterized by field emission scanning electron microscopy (FESEM) LEO SUPRA 55VD ultra-high resolution of Zeiss, Germany. Additionally, the characterization was also done by transmission electron microscope (TEM) FEI Philips CM12 equipped with analySIS Docu Version 3.2 image system of Phillips, Netherland. Electrochemical measurements were carried out on Potentiostat/Galvanostat EG&G Model 273A complete with the Power Suite program of Princeton Applied Research, USA. BSCF modified glassy carbon electrode (or graphene modified glassy carbon electrode), a platinum wire and an Ag/AgCl (3.0 M KCl) served as the working electrode, the auxiliary electrode and the reference electrode, respectively. Electrochemical impedance spectroscopy (EIS) experiments were made using an EG&G FRD 100 with ZSimpWin 3.22 software of Princeton Applied Research, USA at a frequency range of 100 kHz to 100 mHz and AC voltage amplitude 5 mV.

2.2. Synthesis of BSCF powder

BSCF precursor powders were prepared by a sol-gel method. 0.04 mol of ethylenediamminetetraacetic acid (EDTA) was mixed with 1 M of ammonia solution yielding the NH_3-EDTA buffer solution. Nitrate salts of $Ba^{2+,}$ Sr^{2+}, Co^{2+} and Fe^{3+} were dissolved in distilled water to prepare the solution mixture. This was then added to the NH_3-EDTA buffer solution prior to addition of 0.06 mol anhydrous citric acid to form the precursor solution. Ammonia solution was used as pH adjustor to obtain pH 5, 7 and 9. The final solutions were heated at 100 °C and stirred until metal-citrate-nitrate complex was formed. The gelled samples obtained were baked in a drying oven at 250°C for 12 hours before being calcined at 900 °C for 5 hours. The powder produced was then ball-milled for 10 hours.

2.3 Physical Characterization of BSCF powders

The phases present in the calcined BSCF powder were analyzed with powder XRD. Measurements were made with CuKα = 1.54252 Å radiation and 2θ diffraction angles ranging from 20 to 90Å with a current of 40 mA and energy of 40 kV. The thermal decomposition behavior of the precursor gel was studied using themogravimetric analysis in a temperature range of 30–900 °C and a heating rate of 5 °C/min. The specific surface area of calcined powder has been measured using a multi point BET surface area analyzer at the temperature of liquid nitrogen. The specific surface area (S_{BET}), the total pore volume (V_{tot}) and the pore width (D_w) were provided by the manufacturer's software. The morphologies of the calcined and ball-milled powder were observed by a scanning electron microscope with an acceleration voltage of 15kV.

2.4. Preparation of BSCF modified glassy carbon electrode

0.2 g of BSCF powder is dissolved in water. The mixture is then sonicated for 45 minutes until it is homogeneous. A bare glassy carbon electrode is polished with alumina powder and then rinsed ultrasonically with deionized water for 20 minutes. 1 μL of BSCF solution is casted on the surface of the electrode and left to dry at room temperature. The step is repeated with 2, 3, 4 and 5 μL of the solution. Prior to use, the modified electrode was carefully rinsed with water to remove the loosely attached BSCF on the electrode surface.

2.5. Electrochemical Characterization of BSCF

The cyclic voltammetry of 5 mmol L^{-1} $K_3[Fe(CN)_6]$ in 0.1 mol L^{-1} KCl on BSCF/glassy carbon electrode were carried out at potential window of −0.2 V to 0.8 V at room temperature with different scan rates. The electrolyte solution was purged with oxygen free nitrogen gas to eliminate oxygen before use. The EIS measurement was immediately performed after cyclic voltammetry. A sinusoidal signal with amplitude of 5 mV was applied. The modulus and phase were plotted over a frequency range of 100 kHz to 100 mHz.

3. RESULT AND DISCUSSION

The XRD patterns of the BSCF powders synthesized at pH 5, 7 and 9 with the citrate-EDTA method are shown in Fig. 1. It is obvious that a single crystalline phase of BSCF oxide was successfully obtained after calcination. The calcination has to be done at high temperatures i.e. up to 900 °C, to ensure that a single crystalline phase was obtained. At low calcination temperatures, the ‘as synthesized’ black ash is not fully crystallized and is amorphous in nature with some trace quantities of metal oxides associated with the intrinsic tendency of the metal to form carbonates [19]. Sharp lines in the XRD pattern indicate that a well-crystallized structure is formed. All the peaks available indicate a cubic perovskite structure and correspond to the reflection planes (100), (110), (111), (200), (210), (211), (220), (221), and (310). The XRD spectra of BSCF at pH 7 and 9 also show similar crystalline structures. However, the XRD spectra of BSCF pH 5 show that it is poorly crystallized. It can be seen that at pH 5, the 2θ peak appeared at 24.5° which cannot be found for the BSCF formed at pH 7 and pH 9. This peak belongs to an intermediate phase, BaO which has been formed from the decomposition of $BaCO_3$ [20]. A higher calcination temperature might be needed for BSCF at pH 5 to achieve a pure crystalline phase.

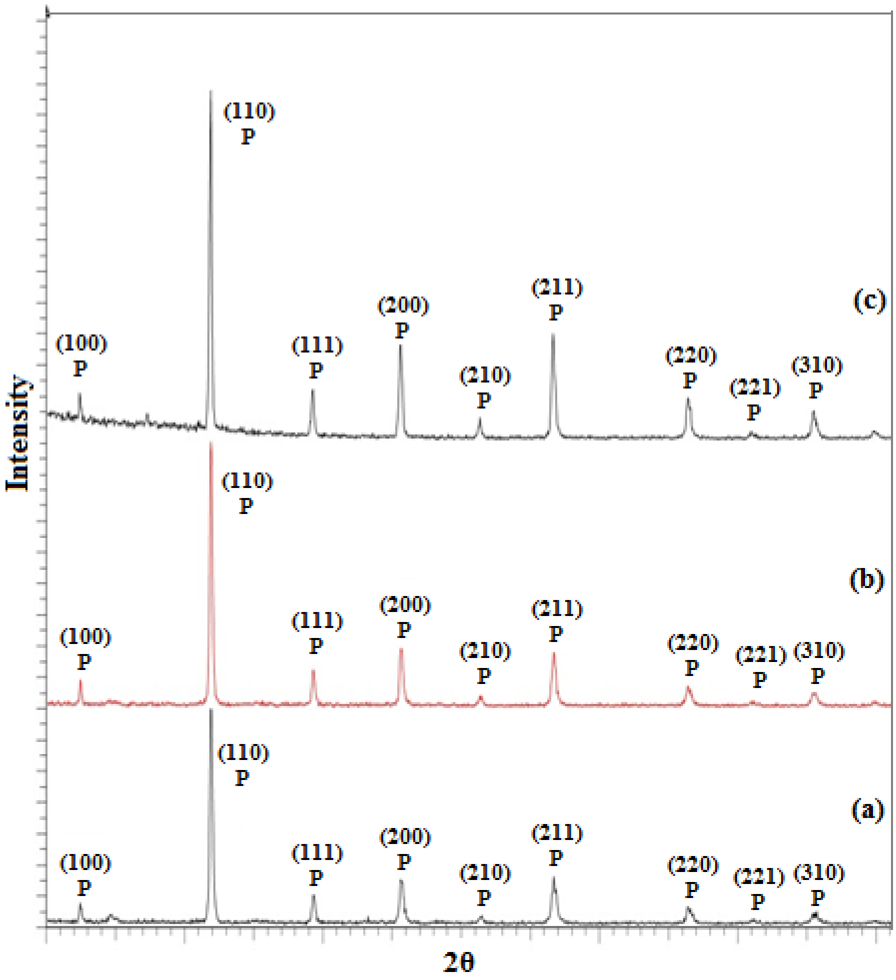

Figure 1. XRD patterns of BSCF powders synthesized by combined citrate-EDTA method at pH (a) 5, (b) 7, and (c) 9.

The pH value of the precursor solution does affect the chelation between the cations and EDTA or citric acid. It has been reported [21] that EDTA is responsible for the complexation with the four metal cations while the citric acid contributes to the gelation and formation of a polymeric network. At higher pH, the EDTA exists in a higher unprotonated form resulting in better complexation of the metal cations. Less efficient crystallization of the BSCF powder occurs at the lower pH. This is the reason why BSCF at pH 5 shows more of the amorphous phase compared to those at the other pH. The spectra of BSCF at pH 9 shows narrow peaks of highest intensity compared to other pH, indicating that the material is highly crystalline. At pH 9, it was reported [22] that the distribution of the HY^{3-} species from EDTA and L^{3-} species of citric acid are at their maximum. Hence, this might be the reason for the highest yield. This fact is also revealed by XRD analysis. From the Debye-Schrrer formula (equation 1), the crystal size of BSCF at pH 5 (34.5 nm), pH 7 (33.1 nm) and pH 9 (37.5 nm) are obtained.

$$D = \frac{0.9\lambda}{(FWHM \times \cos\theta)} \quad \text{....................................(1)}$$

Fig. 2 shows similar patterns for the thermogravimetric (TG) and differential thermogravimmetric (DTG) plots for the samples. During the heating process in N_2 gas, BSCF undergoes a weight loss due to the release of oxygen [23].

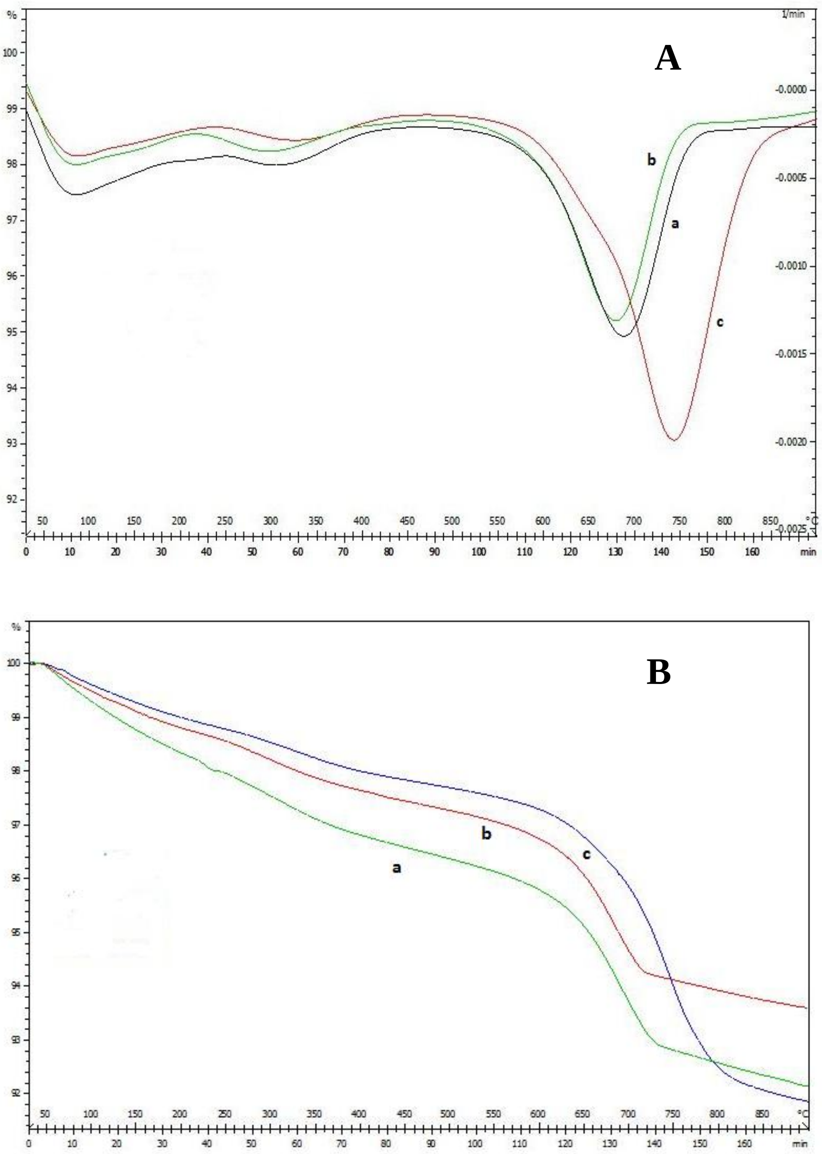

Figure 2. (A) TG and (B) DTG curves of calcined BSCF powders at (a) pH 5, (b) pH 7 and (c) pH 9 at heating rate 5°C min^{-1}.

The small endothermic peak at 100 °C in the TG plot is caused by the loss of the residual and hydrated water as well as other surface contaminants. According to Lee *et al.* [24] the charation of the gelled powders happened at 200 °C but Patra *et al.* [19] has suggested that the exothermic peak at 237 °C is attributed to the combustion of metal/nitrate/citrate/EDTA Since exothermic peaks can be seen in the range between 200 °C to 250 °C, it is worth noting that both reactions do occur. An endothermic peak at 350 °C results from the decomposition of metal-chelates to metal oxides. The DTG plot also shows that a more obvious weight loss starts from 400-600 °C. This means that at this temperature range, BSCF has released oxygen. TGA studies demonstrate that BSCF may be a suitable material for reactions at lower temperatures starting from 400 °C. A more obvious weight loss between 650 °C and 750 °C can be detected due to the thermal decomposition of carbonates [25]. All combustion occurs at a single stage which shows that the complex is stable.

Fig. 3 shows the SEM micrographs of the BSCF powders prepared at different pH. The particle size is in the range of 50 nm to 1 μm which resulted from large layered particles with smaller particulates precipitating on the surface [26]. However, although the range of particle size is wide, the powders arrange themselves uniformly. After ball-milling for 10 hours, the particle size of the BSCF was significantly reduced. But the BSCF does not appear to show a homogeneous particle size distribution. Instead, the microstructure of the BSCF powders are agglomerates and dense. With a 3000X magnification, BSCF at pH 9 appears to be more compact in arrangement than at the other pH. The particle size plays an important role in the adsorption process. Particles with higher surface area allow more gas adsorption to occur. Thus it can be said that BSCF at pH 9 has a greater tendency to adsorb oxygen than BSCF at pH 5 and 7. With a 10000X magnification, BSCF with a porous structure is apparent which supports the adsorption phenomenon expected. The arrangement between the particles is shown to form cavities which may also assist in gas transport. It is noted that the BSCF particles is well contacted to one another.

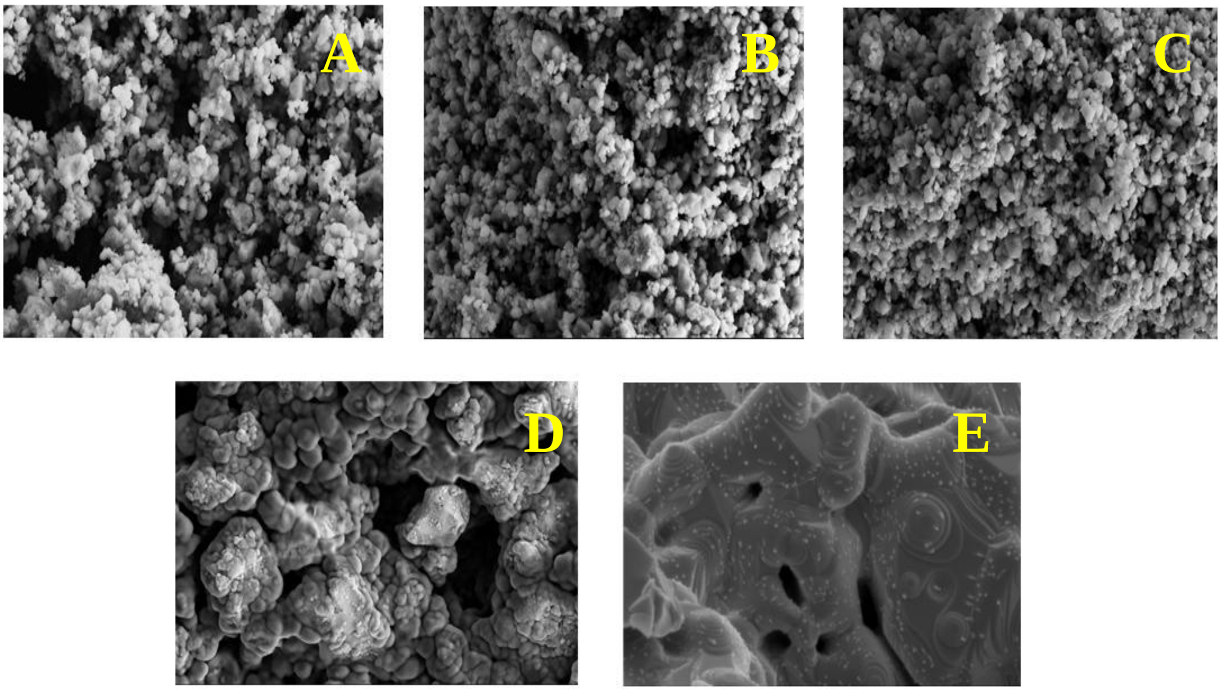

Figure 3. SEM photomicrographs of BSCF powders at (a) pH 5, (b) pH 7 and (c) pH 9 (d) pH 9 at 5000X magnification and (e) pH 9 at 10000X magnification which were calcined at 900°C for 5 hours and ball-milled for 10 hour.

This characteristic is important to ensure better transport of oxygen within the cathode and into the electrolyte solution. It can also be seen that the BSCF has a homogeneous microstructure with porous structure. It has been reported that the cathode microstructure affected the electrochemical activity of the BSCF electrode [27]. Sufficient porosity is important for electrodes in order to allow rapid transport of gaseous reactants and to provide abundant sites for electrochemical reactions in properly designed electrodes. Measurements of adsorption capacity of the BSCF samples at various pH were carried out at 77 K. Fig. 4 A shows that all BSCF samples have a type IV isotherm with IUPAC type H3 hysteresis loop. This is a characteristic of solids which consists of aggregates or agglomerates of particles forming slit shaped pores with non-uniform sizes and shapes. The presence of micropores can be seen by the sudden increase at P/Po < 0.01 which is distinctive to this type of isotherm [28]. However, a larger N_2 adsorption uptake at P/Po < 0.01 can be seen for BSCF at pH 9 which indicates that microporosity is the highest compared to at other pH. The total N_2 adsorption uptake is largest at pH 9 followed by pH 7 and finally at pH 5 in that order. Fig. 4 B shows that in general all BSCF samples have a wide pore size distribution i.e. in the range of 1-10 nm. BSCF at pH 5 has the broadest distribution followed by BSCF at pH 7. Meanwhile BSCF pH 9 shows a much narrower pore size distribution i.e. between 1-5 nm. Based on the pore size distribution, all BSCF samples have both microporous and mesoporous particles. However, such microporosity is not observed in the SEM micrographs. Hence, the BSCF obtained might be classified as small polycrystals which are also known as grain clusters [29].

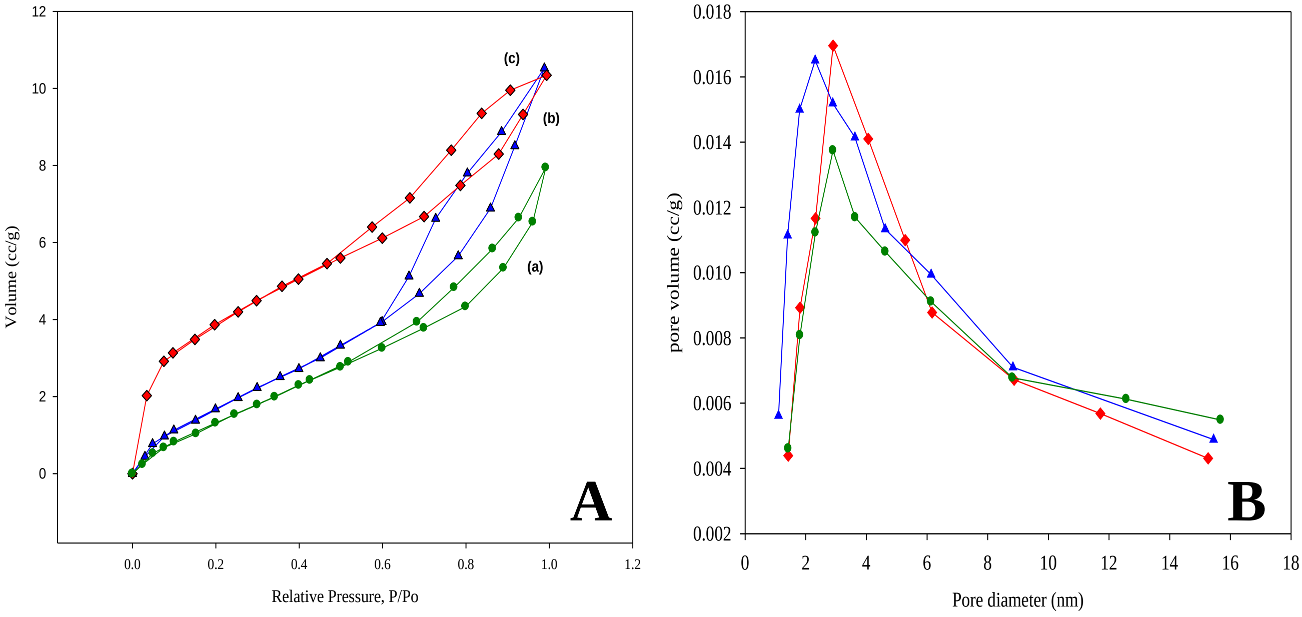

Figure 4. (A) Nitrogen adsorption/desorption isotherms and (B) Pore-size distribution curves of BSCF at (a) pH 5, (b) pH 7 and (c) pH 9.

Table 1 show that BSCF at pH 9 displays the highest BET and V_{tot} but with the smallest pore size (D_w). It is concluded that BSCF samples may be classified as mesopores based on its sizes. However, the Langmuir surface area data shows a slightly different result where the value increases with increasing pH. Since the Langmuir surface area is calculated on area covered by one layer of gas, it can be considered that the monolayer increases with the increase in pH. All BSCF samples follow the same trends in total adsorption-desorption pore diameter in which desorption pore diameters are smaller compared to the adsorption pore diameters. BSCF prepared at pH 9 have a greater tendency of adsorption as strength of a porous material depends directly on the total pore volume.

Table 1. BSCF at various pH

pH of adsorbent	S_{BET} (m^2g^{-1})	Pore size, D_w (nm)	Adsorption pore diameter (nm)	Desorption pore diameter (nm)	Pore volume (cm^3g^{-1})	Langmuir surface area (m^2g^{-1})
5	6.1	7.4	3.0	2.3	0.011	35.6
7	6.5	7.6	2.3	2.2	0.012	48.9
9	14.4	4.5	1.8	1.4	0.016	42.6

From the phase, thermal and surface morphological characterization, BSCF at pH 9 is considered as the best pH and is used for further characterization. The electrochemical characterization of BSCF electrode is used to determine; (a) electron transfer/mass transport, (b) diffusion control and (c) capacitance behaviour. The volume of BSCF solution plays an important role as it will influence the surface area of the electrode (Fig. 5). It appears that with an increase in BSCF volume, the current density increases which indicates easier electron transfer within the system. But the anodic current remains almost constant after 5 µL of BSCF solution is used. This shows that electron transfer is already stable at 5 µL of BSCF. Thus this is the optimum volume as too much BSCF solution will take longer to dry up.

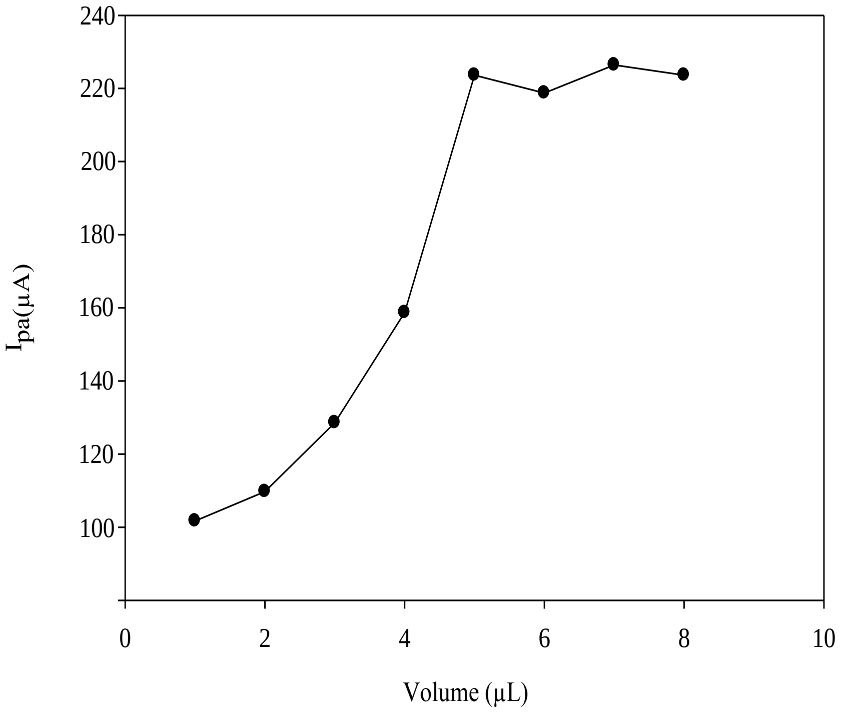

Figure 5. Volume of BSCF solution vs. anodic peak current

Fig. 6 shows cyclic voltammograms (CV) where the anodic peak current varies with the volume of BSCF used which indicates the catalytic effects on the 5.0 mmol L^{-1} $K_4[Fe(CN)_6]$ in 0.1 mol L^{-1} KCl as well as the kinetic properties of the bare glassy carbon electrode and BSCF modified glassy carbon electrode. Modification of the glassy carbon electrode gives higher peak currents compared to that with the bare glassy carbon. It shows that addition of BSCF improves the characteristics of the electrode by providing easier electronic transfer on the surface. With the increased amount of BSCF, the surface area for the reaction also increases allowing more electron transfer to occur thus increasing the reversibility of the system. Both oxidation and reduction peaks appear sharp and fairly symmetric with peak separations (ΔE_p) of less than 200 mV indicating good reversibility of the electrode processes. The reversibility is confirmed as all systems with various BSCF volumes have ratios of I_{pa}/I_{pc} equal to unity.

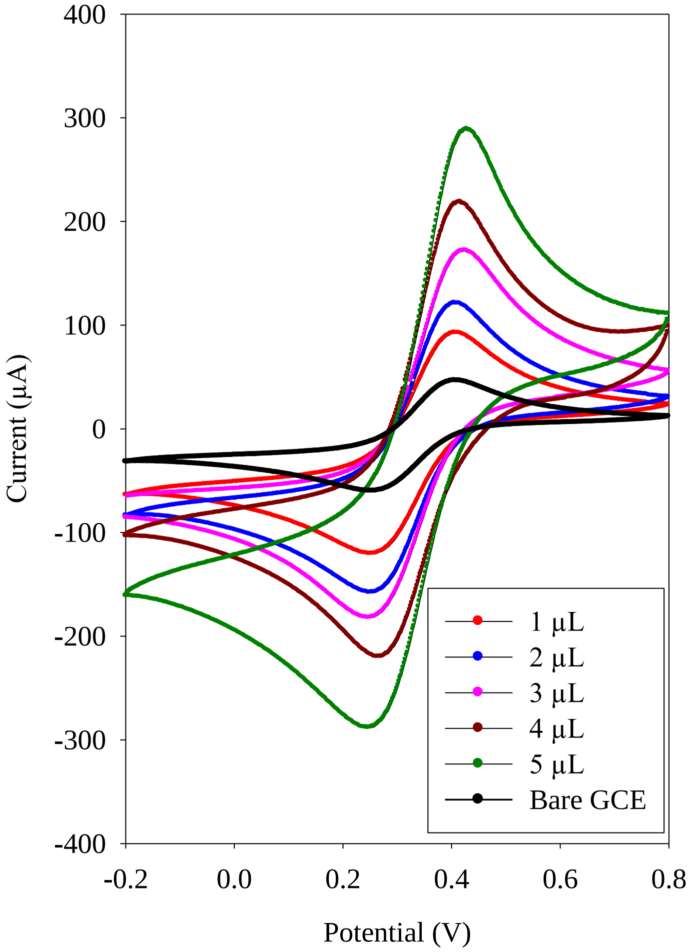

Figure 6. CV of 5.0 mmol L^{-1} $K_4[Fe(CN)6]$ in 0.1 mol L−1 KCl at BSCF electrode. Scan rate is 50 mV s^{-1}.

Fig. 7 shows the effect of scan rate on the BSCF electrode. A linear relationship between scan rate and peak current indicates a surface controlled process [30]. The inset shows that the slope of peak current against the square root of scan rate at around 0.5 which illustrates that the electrode process is diffusion-controlled [31]. This process is controlled by the diffusion rate of reactants towards the electrode surface rather than reaction itself, i.e. kinetic control [32]. These results supported the notion that the $Fe(CN)^{4-}$ reaction is related only to diffusion rate of $Fe(CN)^{4-}$ from solution to the surface of the BSCF electrode. It means that $Fe(CN)^{4-}$ will not remain attached to the BSCF electrode. It will immediately separate from the electrode after reaction. Because of this property the sensitivity of the BSCF electrode will not be decreased.

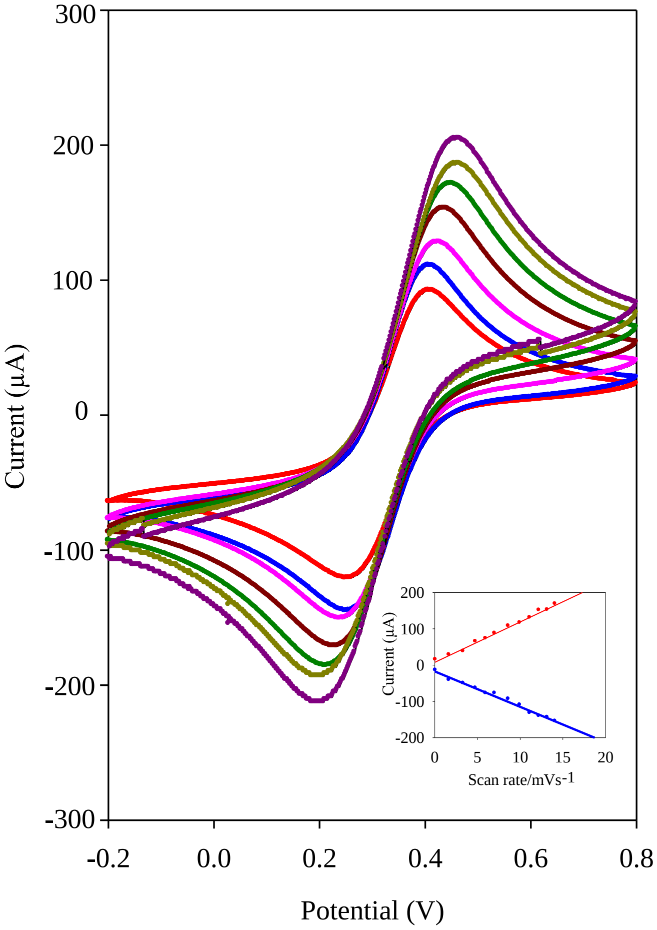

Figure 7. Effect of scan rate on the CV of the 5.0 mmol L^{-1} $K_4[Fe(CN)6]$ in 0.1 mol L^{-1} KCl at 50, 75, 100, 125, 150, 175 and 200 mV s-1. Inset: the plot of peak currents vs. the square root of scan rate.

From Table 2 we can see that the correlation coefficient R^2 is almost unity with the increase in the volume of BSCF solution used. This suggests that the increased amount of BSCF will ease the control of electron transfer and mass transport thus improving the diffusion process. Overall, the peak separation decreased with the increase in the BSCF solution volume. But, as the scan rate increase, the E_{pa} shifts towards positive potentials and the E_{pc} shifts toward negative potentials, making the ΔE_p values larger which indicate that the process is quasi-reversible and dependent on charge transfer [33]. With increasing scan rate, I_{pa} and I_{pc} also increase which may due to the increase in the rate of electron transfer. This suggests that this process occurs at higher rate of charge electron transfer.

Table 2. The relationship between peak current and the square root of scan rate

Vol	ν	$\nu^{1/2}$	Peak Current (μA)		$R^2 I_{pa}$ *vs* $\nu^{1/2}$	$R^2 I_{pc}$ *vs* $\nu^{1/2}$	Slope (I_{pa})	Slope (I_{pc})	E_{pa} (mV)	E_{pc} (mV)	ΔE
			Anodic	Cathodic							
1	50	7.07	86.5	78.8	0.98	0.98	1.01	1.17	409.7	253.5	156.2
	75	8.66	106.5	94.6					410.0	256.1	153.9
	100	10.00	115.3	111.0					420.5	245.8	174.7
	125	11.18	129.4	132.9					435.3	231.0	204.3
	150	12.25	150.0	141.1					447.2	222.2	225.0
	175	13.23	150.7	145.5					462.0	204.0	258.0
	200	14.14	167.5	156.1					460.3	199.7	260.6
2	50	7.07	115.7	106.0	0.98	0.99	1.21	1.19	408.5	256.1	152.5
	75	8.66	138.0	127.4					411.7	257.5	154.2
	100	10.00	151.9	138.0					425.6	243.8	181.8
	125	11.18	176.3	163.4					437.3	233.9	203.4
	150	12.25	195.3	181.0					449.2	215.9	233.3
	175	13.23	197.5	190.5					461.1	202.3	258.9
	200	14.14	222.3	207.1					466.7	222.5	278.1
3	50	7.07	153.8	137.2	0.99	0.99	1.23	1.20	423.6	249.8	173.8
	75	8.66	177.5	159.9					431.3	247.8	183.5
	100	10.00	194.1	176.5					441.3	231.9	209.4
	125	11.18	204.6	184.6					449.2	229.6	219.7
	150	12.25	218.6	192.9					449.2	225.9	223.3
	175	13.23	227.6	209.3					468.9	214.2	254.6
	200	14.14	243.0	221.2					466.9	208.3	258.6
4	50	7.07	203.4	168.2	0.99	0.93	2.37	2.15	413.7	271.4	142.3
	75	8.66	238.6	194.1					421.6	263.4	158.2
	100	10.00	257.0	214.7					421.6	265.1	158.3
	125	11.18	275.8	219.5					435.3	261.5	173.8
	150	12.25	291.5	291.5					447.2	247.8	199.4
	175	13.23	313.6	296.1					449.2	243.8	205.4
	200	14.14	337.0	311.2					453.2	239.8	213.4
5	50	7.07	260.1	203.7	0.95	0.96	2.53	2.51	429.3	253.5	175.8
	75	8.66	290.2	233.5					441.3	243.5	197.7
	100	10.00	285.4	230.3					439.3	243.5	195.7
	125	11.18	319.7	270.3					456.9	219.9	237.0
	150	12.25	343.4	291.6					466.9	217.9	249.0
	175	13.23	364.4	310.3					472.8	205.9	266.9
	200	14.14	376.3	331.6					484.5	196.3	288.2

In order to further characterize the electrochemical properties of BSCF modified electrode, the AC impedance spectra were measured. This technique is very sensitive to the state of the interface and is used to characterize electrode processes and complex interfaces. This method is based on the application of an AC potential ($E(t) = E_o \cos(\omega + t)$) of small amplitude. As a consequence, an AC current is obtained, $I(t) = I_0 \cos(\omega t - \varphi)$. From the relation of both signals, the impedance (Z) is obtained ($Z = E(t)/I(t)$). The measurements are carried out at different AC frequencies and thus the name of impedance spectroscopy. Impedance methods allow characterizing the double layer interface at the electrodes and the physicochemical processes of widely differing time constants, sampling electron transfer at high frequency and mass transfer at low frequency. Figure 8(A) shows fitted Randle modified equivalent circuit model for the impedance spectra.

The Nyquist plot is the function impedance one can express it in terms of a complex number ($Z = Z_{real} + j\, Z_{imag}$) and plot the Z_{real} vs Z_{imag}. As depicted in Fig. 8(B), the BSCF exhibited a diffusion controlled electrode process. The effect of diffusion appears at low frequencies in the complex plane plot as a straight line 45° to the real axis, as shown for all volumes of BSCF solution. When diffusion effects are present in electrochemical systems, the equivalent circuit is modified by the inclusion of a diffusion component, known as the Warburg impedance. The charge transfer resistance is lower with 5 μL volume.

The R_{ct} value is usually used as a response parameter. With the increase in volume, the R_{ct} value of the BSCF electrode decreased. This phenomenon could be interpreted that the positive charges of the BSCF electrode could attract the negatively charged $[Fe(CN)_6]^{3-/4-}$ redox couple, facilitate the electron transport between the interface and decrease the EIS value [34] . There is lower resistance when more of the BSCF surface exposed is exposed for reactionThe R_{ct} value is inversely proportional to the rate of electron transfer.

The apparent standard rate constant (k_{app}) values of the electrodes were calculated from Eq. (2) [35];

$$k_{app} = \frac{RT}{\eta^2 F^2 A R_{ct} C} \text{..} (2)$$

where A is the area of the electrode, C is the concentration of the $[Fe(CN)_6]^{4-/3-}$, and R, T, n and F are their usual meanings. The calculated data are shown in Table 3. For the higher volume of BSCF, the electron transfer processes at the interfacial layer are easier since the k_{app} value is bigger. These results also agree with the results of the cyclic voltammetric studies.

Another way to represent the impedance results is by using the Bode plot where the modulus of the impedance ($\log |Z|$) and the phase angle (φ) between the AC potential and the AC current as a function of the frequency ($\log \omega$) are plotted (Fig. 8 C). In this plot, the impedance data which are frequency independent represent the behavior of the resistive processes whereas the ones that are dependent on the frequency are more related to capacitive or diffusive processes. From the plot, the BSCF electrode shows resistive behaviour at low frequency and changes to capacitive behaviour at high frequency. The same trend spotted at all five different volume of BSCF. Meanwhile, according to the study of Mansfeld [36], the occurrence of the so-called low-frequency Warburg impedance in this study may indicate that the anodizing processes is controlled by a diffusion process.

In the bode magnitude (Fig. 8D), there is one peak in the maximum phase angle i.e., one relaxation process. This result indicates that one charge transfer process is taking place at the interface at different potential values. This process may be diffusion or adsorption [37]. BSCF solution with the highest volume show the most capacitive behaviour compared to other.

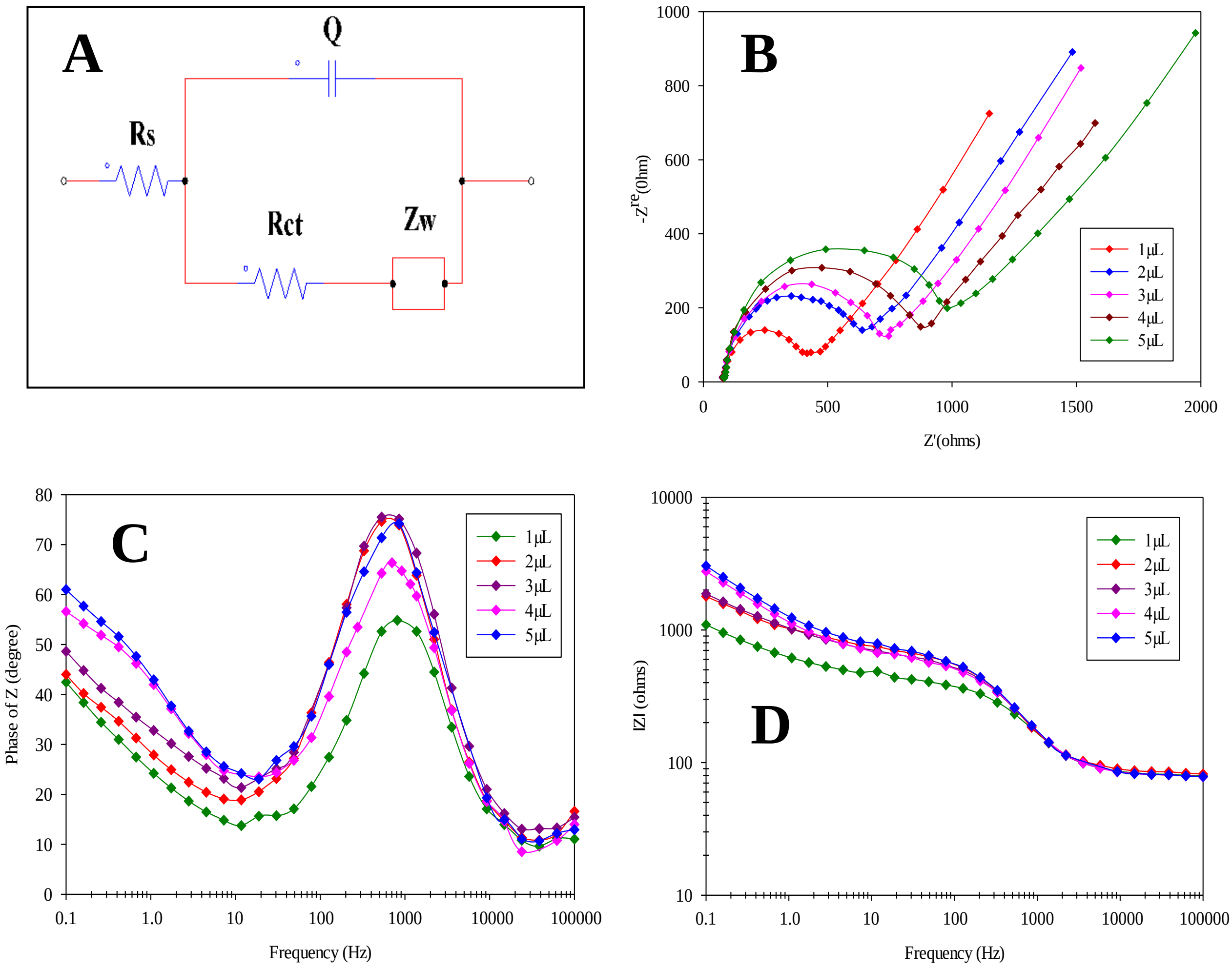

Figure 8. (A) Modified Randles equivalent electrical circuit, (B) Nyquist plot (C) Bode phase and (D) Bode magnitude plots obtained for the various BSCF solution volume in 5mm $[Fe(CN)_6]^{4-/3-}$ and 0.1 mol L^{-1} KCl at 0.5 V

Table 3. Apparent constant value for BSCF solution with different volume.

Volume	R_S/Ωcm2	Rct/Ωcm2	K_{app} (10^{-7})
1	88.06	547	4.41
2	83.65	499.6	4.58
3	82.04	488.2	4.6
4	77.94	402.2	5.3
5	82.12	307.9	7.3

A higher BSCF volume means a higher surface area exposed for the reaction thus increasing the capacitance. The capacitance value is linear to a given potential window. From the CV results (data is not shown) the increase in amount will increase the potential window. Therefore, the largest area of potential window in 5 µL of BSCF solution give the largest capacity compared to other volume. Fig. 9 shows the variation of calculated specific capacitance (F/g) versus the different scan rate. These results show that the efficiency of BSCF 5 µL is at its highest. This result also supports the EIS data obtained.

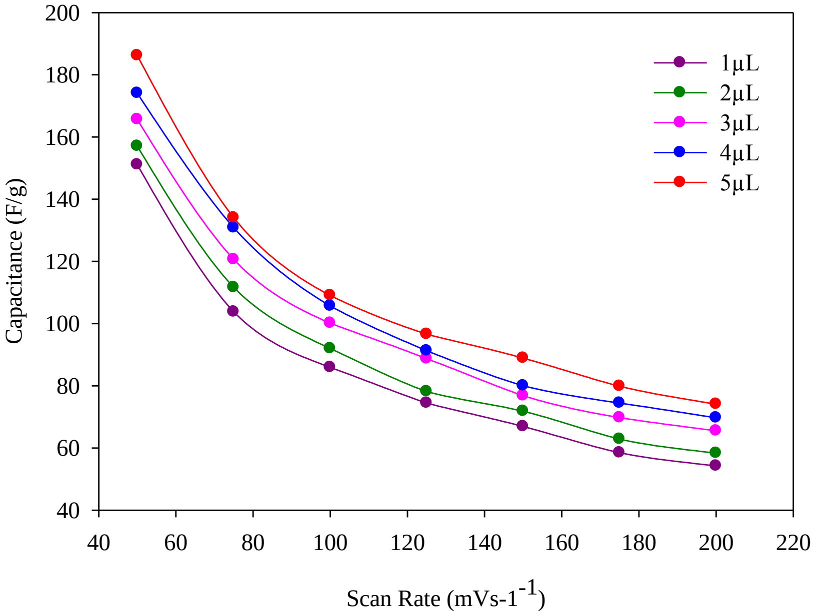

Figure 9. Plot of capacitance *vs.* scan rate for different volumes of BSCF solution

4. CONCLUSION

The effect of solution pH is an important parameter for controlling the BSCF oxides powder characteristics synthesized by the EDTA–citrate method. The BSCF at pH 9 with 5 µL volume is the optimum condition for better material characteristics. The phase formation behavior of BSCF is a complex process and different in every pH tested. Morphology studies show that the particle properties are mostly coarse and agglomerate. A good theoretical correlation between pore sizes, volumes and surface area is obtained. The BSCF oxides are capable of releasing oxygen at 400 °C. The BSCF cathode displays diffusion controlled electrode process. Facile electron transfer is observed when high amounts of BCSF are used as an electrode.

ACKNOWLEDGMENT
This work was supported by the Ministry of Higher Education (MOHE) Fundamental Research Grant Scheme (FRGS) 203/PKIMIA/6711263 and Universiti Sains Malaysia Incentive Postgraduate Grant, 1001/PKIMIA/821014. One of the authors (FY) would like to acknowledge Universiti Malaysia Terengganu, Malaysia for the study leave rendered.

References

1. Z.P. Shao, S.M. Haile, *Nature* 431 (2004) 170
2. A. Leo, S. Liu, J.C. Diniz da Costa, Z. Shao, *Sci. Technol. Adv. Mater.* 7 (2006) 819
3. H.J.M. Bouwmeester, *Catal. Today* 82 (2003) 141
4. Z.P. Shao, G.X. Xiong, H. Dong, W.S. Yang, L.W. Lin, *Sep. Purif. Technol.* 25 (2001) 97
5. X. Sun, S. Li, J. Sun, X. Liu, B. Zhu, *Int. J. Electrochem. Sci.* 2 (2007) 462
6. A. Subramania, T. Saradha, S. Muzumathi, *J. Power Sources* 165 (2007) 728
7. B.Liu, Y. Zhang, *J. Alloy Compound*. 453 (2008) 418
8. H. Zhao, F. Mauvy, C. Lalanne, J.M. Bassat, S. Fourcade, J.C. Grenier, *Solid State Ionics* 179 (2008) 2000
9. A. Princivalle, E. Djurado, *Solid State Ionics* 179 (2008) 1921
10. V.B. Vert, J.M. Serra, *Fuel Cells* (2009) 663
11. Y. Li, R. Gemmen, X. Liu, *J. Power Sources*. 195 (2010) 3345
12. S. Shimizu, T. Yamaguchi, Y. Fujishiro, *ECS Trans.* 25 (2009) 975
13. Z. Chen, R. Ran, W. Zhou, Z. Shao, S. Liu, *Electrochim. Acta* 52 (2007) 7343
14. Z. Shao, G. Xiong, J. Tong, H. Dong, W. Yang, *Sep. Purif. Technol*. 25 (2001) 419
15. Z. Shao, W.Y. Cong, H. Dong, J. Tong, *J. Membr. Sci.* 172 (2000) 177
16. W. Zhou, R. Ran, Z. Shao, R. Cai, W. Jin, N. Xu, J. Ahn, *Electrochim. Acta* 53 (2008) 4370
17. W. Zhou, Z. Shao, R. Ran, Z. Chen, P. Zeng, H. Gu, W. Jin, N. Xu, *Electrochim. Acta* 52 (2007) 6297
18. Z. Wu, W. Zhou, W. Jin, N. Xu, *AIChE J.* 52 (2006) 769
19. H. Patra, S.K. Rout, S.K. Pratihar, S. Bhattacharya, *Powder Technol*. 209 (2011) 98
20. Z. Pingying, C. Zhihao, Z. Wei, G. Hongxia, S. Zongping, L. Shaomin, *J. Membr. Sci 291* (2007) 148
21. A. Feldhoff, M. Arnold, J. Marynczuk, H. Wang, *Solid State Sci*. 10 (2008) 689
22. A. Tschöpe, S. Kilassonia, R. Birringer, *Solid State Ionics* 173 (2004) 57
23. S. Faraji, K.J. Nordheden, S.M. Stagg-Williams. *Appl. Catal. B Environ*. (2010) 118
24. S. Lee, Y. Lim, E.A. Lee, H.J. Hwang, J. Woong, *J. Power Sources* 157 (2006) 848
25. S. Liu, M. Liu, Z. Shao, J.C. Diniz da Costa, Z.P. Xu. *J. Am. Ceram. Soc*. 90 (2007) 84
26. M. Darab, M. S. Toprak, G. E. Syvertsen,M. Muhammed, *J. Electrochemi. Soc* 156 (2009) 139
27. Q.L. Liu, K.A. Khor, S.H. Chan, *J. Power Sources* 161 (2006) 123
28. K. Inomata, Y. Otake, *Micropor. Mesopor. Mater* 143 (2011) 60
29. Z M. Zhou, Z. Wei, H. Qiao,L, Zhu, H. Yang, T. Xia, *J. Nanomater*. 2009 (2009)1-5.
30. E. Laviron, *J. Electroanal. Chem* 101 (1979)19
31. A.J. Bard, L.R. Faulkner, *Electrochemical Methods*, Wiley, New York, 1980.
32. J. R. Selman, C. W.Tobias, *Adv. Chem. Eng*. 10 (1978) 211
33. S.A. Kumar, S.M. Chen, *Sensors* 8 (2008)739
34. Z. Zhanxia, Z. Hui, W.Xiaolei, Y. Xiurong, Microchim Acta 174 (2011)183–189.
35. 35 .D. Raistrick, D.R. Franceschetti, J.R. Macdonald, E. Barsoukov, *Impedance Spectroscopy: Theory Experiment, and Applications*, Wiley, New Jersey, 2005.
36. F. Mansfeld, *Corrosion,* 36 (1981) 301
37. S.A.M. Refaey, G. Schwitzgebel, *Appl. Surf. Sci.* 135 (1998) 243